
Molecular Geometry Pretraining with SE(3)-Invariant Denoising Distance Matching

Shengchao Liu

Mila - Québec AI Institute
Université de Montréal

Hongyu Guo

National Research Council Canada
University of Ottawa

Jian Tang

Mila - Québec AI Institute
HEC Montréal
CIFAR AI Chair

Abstract

Pretraining molecular representations is critical in a variety of applications in drug and material discovery due to the limited number of labeled molecules, yet most of existing work focuses on pretraining on 2D molecular graphs. The power of pretraining on 3D geometric structures, however, has been less explored, owing to the difficulty of finding a sufficient proxy task to empower the pretraining to effectively extract essential features from the geometric structures. Motivated by the dynamic nature of 3D molecules, where the continuous motion of a molecule in the 3D Euclidean space forms a smooth potential energy surface, we propose a 3D coordinate denoising pretraining framework to model such an energy landscape. Leveraging a SE(3)-invariant score matching method, we propose SE(3)-DDM where the coordinate denoising proxy task is effectively boiled down to the denoising of the pairwise atomic distances in a molecule. Our comprehensive experiments confirm the effectiveness and robustness of our proposed method. The source codes of this paper are released on [GitHub](#).

1 Introduction

Learning effective molecular representations is critical in a variety of tasks in drug and material discovery, such as molecular property prediction [13, 18, 69], *de novo* molecular design and optimization [6, 49, 71], and retrosynthesis and reaction prediction [20, 48, 59]. Recent work based on graph neural networks (GNNs) [18] has shown superior performance thanks to the simplicity and effectiveness of GNNs in modeling graph-structured data. However, the problem remains challenging due to the limited number of labeled molecules as it is general expensive and time-consuming to label molecules, which usually requires expensive physics simulations or wet-lab experiments.

As a result, recently, there is growing interest in developing pretraining or self-supervised learning methods for learning molecular representations by leveraging the huge amount of unlabeled molecules [26, 33, 33, 58, 70]. These methods have shown superior performance on many tasks, especially when the number of labeled molecules is insufficient. One limitation of these approaches is, however, that they represent molecules as topological graphs and molecular representations are learned through pretraining 2D topological structures (*i.e.*, based on the covalent bonds). But intrinsically, for molecules, a more natural representation is their 3D geometric structures, which largely determine the corresponding physical and chemical properties. Indeed, recent work [18, 34] has empirically verified the importance of applying 3D geometric information for molecular property prediction tasks. Therefore, a more promising direction is to pretrain molecular representations based on their 3D geometric structures, which is the main focus of this paper.

The main challenge for molecule geometric pretraining arises from discovering an effective proxy task to empower the pretraining to extract essential features from the 3D geometric structures.

Our proxy task is motivated by the following observations. Studies [43] have shown that molecules are not static but in a continuous motion in the 3D Euclidean space, forming a potential energy surface (PES). As shown in Fig. 1, it is desirable to study the molecule in the local minima of the PES, called *conformer*. However, such stable state conformer often comes with different noises for the following reasons. First, the statistical and systematic errors on conformation estimation are unavoidable [10]. Second, it has been well-acknowledged that a conformer can have vibrations around the local minima in PES. Such characteristics of the molecular geometry motivate us to attempt to denoise the molecular coordinates around the local minima, to mimic the computation errors and conformation vibration within the corresponding local region. The denoising goal is to learn molecular representations which are insensitive to such noises and effectively capture the energy surface around the local minima.

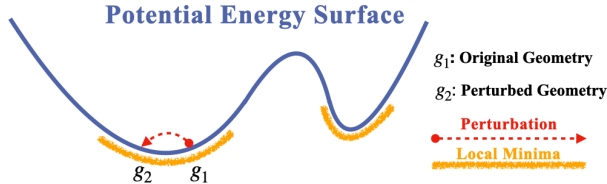


Figure 1: Illustration on coordinate geometry of molecules. The molecule is in a continuous motion, forming a potential energy surface (PES), where each 3D coordinate (x-axis) corresponds to an energy value (y-axis). The provided molecules, *i.e.*, conformers, are in the local minima (g_1). It often comes with noises around the minima (*e.g.*, statistical and systematic errors or vibrations), which can be captured using the perturbed geometry (g_2).

To achieve the aforementioned goal, we propose a pretraining framework, coined SE(3)-Denoising Distance Matching (SE(3)-DDM). In detail, to capture the smooth energy surface around the local minima, SE(3)-DDM aims to maximize the mutual information (MI) between the original geometry and its perturbed version (*i.e.*, g_1 and g_2 in Fig. 1). In practice, it is of course difficult to directly maximize the mutual information between two random variables. We instead propose to maximize the lower-bound of the mutual information, which amounts to denoise the perturbed structure into the original one. Directly denoising the noisy coordinates, however, remains challenging because one may need to effectively constrain the pairwise atomic distances while changing the atomic coordinates. To cope with this issue, we further leverage a SE(3)-invariant score matching method to successfully convert the coordinate denoising desire to the denoising of pairwise atomic distances, which then can be effectively computed. In other words, our pretraining proxy task effectively boils down to achieving an intuitive learning objective: denoising a molecule’s pairwise atomic distances. We empirically verify, using 22 downstream geometric molecular prediction tasks, that our method outperforms eight state-of-the-art pretraining baselines.

Our main contributions are summarized as follows. (1) We propose a novel coordinate denoising method for molecular geometry pretraining, which to the best of our knowledge is the first to only utilize 3D molecular data for pretraining. (2) To overcome the challenge of attaining the coordinate denoising objective, we introduce a SE(3)-invariant score matching strategy to successfully transform such objective into the denoising of pairwise atomic distances, which can be effectively computed. (3) We empirically confirm the effectiveness and robustness of our proposed method, SE(3)-DDM.

2 Related Work

2.1 Equivariant Geometric Molecule Representation Learning

Geometric Representation Learning. Recently, the 3D geometric representation learning has been widely explored in the machine learning community, including but not limited to 3D point clouds [7, 39, 50, 62], N-body particle [40, 42], and 3D molecular conformation [5, 29, 30, 36, 45, 46, 51], amongst many others. The learned representation should satisfy the physical constraints, *e.g.*, it should be equivariant or invariant to the transition on the Euclidean space. Such constraints can be categorized into the group symmetry as introduced below.

SE(3)-Invariance Energy. Constrained by the physical nature of 3D data, an intriguing principle we need to follow is to learn a SE(3)-equivariant representation. The SE(3) is the special Euclidean group consisting of rigid transformations in the 3D Cartesian space, where the transformations include all the combinations of translations and rotations. Thus, the learned representation will be equivariant to translations and rotations. We also note that for some specific tasks like molecular chirality [1], the representation needlessly satisfy the reflection equivariance. For more rigorous discussion, please check [16, 60]. In this work, we will design a SE(3)-invariant energy function based on a SE(3)-equivariant representation backbone model.

2.2 Self-Supervised Learning for Molecule Representation Learning

In general, there are two categories of self-supervised learning (SSL) [35, 37, 66, 67]: contrastive and generative, and the main difference is if the supervised signals are constructed in an inter-data or intra-data manner. To be more concrete, contrastive SSL extracts two views from the data and designs the supervised signals by detecting if the sampled view pairs are from the same data, and generative SSL learns structural information by reconstructing partial information from the data itself.

2D Molecular Graph (Topology) Self-Supervised Learning. Currently, one of the mainstream research lines for molecule pretraining is on the 2D molecular graph. It treats the molecules as 2D graph, where atoms and bonds are nodes and edges respectively. It then carries out a pretraining task by either detecting if the two augmentations (e.g., neighborhood extraction, node dropping, edge dropping, etc) correspond to the same molecular graph [26, 58, 70] or if the representation can successfully reconstruct the masked subgraph in an auto-encoding manner [26, 27, 33].

3D Molecular Graph (Geometry) Self-Supervised Learning. As the increasing interest on the 3D geometric representation learning, there has been some initial explorations [15, 34] involving the geometric SSL for molecules. GraphMVP [34] introduces an extra 2D topology and employs detection and reconstruction tasks simultaneously between 2D and 3D graphs, yet it focuses on 2D downstream tasks. ChemRL-GEM [15] designs a novel model using both the 2D and 3D molecular graphs. In terms of SSL, it utilizes the geometry information by taking the distance prediction and angle prediction as the generative pretraining tasks. Some of their geometric SSL tasks will be used as baselines in our work, yet we want to highlight that our work is focusing on the pure 3D geometric data without the covalent bonds (2D topology). To the best of our knowledge, our work is the first to explicitly do SSL on pure 3D geometry along the molecule representation learning research line.

3 Preliminaries

Molecular Geometry Graph. Molecules can be naturally featured in a geometric formulation, *i.e.*, all the atoms are in spatially located in 3D Euclidean space. Note that the covalent bonds are added heuristically by expert rules, so they are only applicable in 2D topology graph not 3D geometry graph. Besides, atoms are not static, but in a continual motion along a potential energy surface [2]. The 3D structures at the local minima on this surface are named *conformer*, as shown in Fig. 1. Conformers at such equilibrium state possess nice properties and we would like to model them during pretraining.

Geometric Neural Network. For notation, we denote each conformer as $\mathbf{g} = (X, R)$. Here $X \in \mathbb{R}^{n \times d}$ is the atom attribute matrix and $R \in \mathbb{R}^{n \times 3}$ is the atom 3D-coordinate matrix, where n is the number of atoms and d is the feature dimension. The corresponding representations for the i -th node and whole molecule are:

$$h_i = \text{GNN-3D}(T(\mathbf{g}))_i = \text{GNN-3D}(T(X, R))_i, \quad h = \text{READOUT}(h_0, \dots, h_{n-1}), \quad (1)$$

where T is the transformation function like atom masking, and READOUT is the readout function. In this work, we take the mean over all the node representations as the readout function.

Energy-Based Model and Denoising Score Matching. Energy-based model (EBM) is a flexible tool for modeling the underlying data distribution in the form of Gibbs distribution as $p_\theta(\mathbf{x}) = \exp(-E(\mathbf{x}))/A$, where $p_\theta(\mathbf{x})$ is the model distribution, A is the normalization constant and it is intractable due to the high cardinality of the data space. Recently, there has been various progress in solving this intractable function, including contrastive divergence [11], noise contrastive estimation [23], and score matching (SM) [28, 55, 56]. Specifically, SM solves this by introducing a novel concept, score: it is the gradient of the log-likelihood with respect to the data. SM then matches the model score and data score using Fisher divergence. Further along this research line, denoising score matching (DSM) [64] combines SM with denoising auto-encoding. The main advantage of DSM is that it is equivalent to SM yet with a computationally feasible and efficient solution. In this work, we will explore how DSM can be applied for molecule geometry representation learning by utilizing the distance information, one of the most fundamental factors in geometric data.

Problem Setup. Our goal here is to apply a self-supervised pretraining algorithm on a large molecular geometric dataset, and adapt the pretrained representation for fine-tuning on geometric downstream tasks. For both the pretraining and downstream tasks, only the 3D geometric information is available, and our solution is agnostic in terms of the backbone geometric neural network.

4 SE(3)-Invariant Denoising Distance Matching

This section introduces our proposed SE(3)-DDM. We start with exploring the coordinate perturbation for molecular data in Sec. 4.1. Then we propose a coordinate-aware MI maximization formula and turn it into a coordinate denoising problem in Sec. 4.2. However, the coordinate denoising is non-trivial, since it requires the geometric data reconstruction, and we adopt the score matching for estimation, as introduced in Sec. 4.3. The ultimate training objective is illustrated in Sec. 4.4.

4.1 Coordinate Perturbation for Geometric Data

The mainstream self-supervised learning community designs the pretraining task by defining multiple views from the data, and these views share common information to some degree. Thus, by designing generative or contrastive task to maximize the mutual information (MI) between these views, the pretrained representation can encode certain key information. This will make the representation more robust and can be more generalizable to downstream tasks. In our work, we propose SE(3)-invariant denoising distance matching (SE(3)-DDM), a self-supervised learning (SSL) method for molecule geometric representation learning.

The 3D geometric information, or the atomic coordinates are critical to molecular properties. We also carry out an ablation study to verify this in Appendix B. Then based on this acknowledgement, we propose a geometry perturbation, which adds small noises to the atom coordinates. For notation, following Sec. 3, we define the original geometry graph and an augmented geometry graph as two views, denoted as $\mathbf{g}_1 = (X_1, R_1)$ and $\mathbf{g}_2 = (X_2, R_2)$ respectively. The augmented geometry graph can be seen as a coordinate perturbation to the original graph with the same atom types, *i.e.*, $X_2 = X_1$ and $R_2 = R_1 + \epsilon$, where ϵ is drawn from a normal distribution.

4.2 Coordinate Denoising with Mutual Information Maximization

The two views defined above share certain common information. By maximizing the mutual information (MI) between them, we expect that the learned representation can better capture the geometric information and is insensitive to noises and thus can generalize well to the target downstream tasks. To maximize the MI, we turn to maximizing the following lower bound on the two geometry views:

$$I(G_1; G_2) = \mathbb{E}_{p(\mathbf{g}_1, \mathbf{g}_2)} \left[\log \frac{p(\mathbf{g}_1, \mathbf{g}_2)}{p(\mathbf{g}_1)p(\mathbf{g}_2)} \right] \geq \frac{1}{2} \mathbb{E}_{p(\mathbf{g}_1, \mathbf{g}_2)} \left[\log p(\mathbf{g}_1|\mathbf{g}_2) + \log p(\mathbf{g}_2|\mathbf{g}_1) \right] \triangleq \mathcal{L}_{\text{MI}}. \quad (2)$$

In Eq. (2), we transform the MI maximization problem into maximizing the summation of two conditional log-likelihoods. In addition, these two conditional log-likelihoods are in the mirroring direction, and such symmetry can reveal certain nice properties, *e.g.*, it highlights the equal importance and uncertainty of the two views and can lead to a more robust representation of the molecule.

To solve Eq. (2), we introduce using the energy-based model (EBM) for estimation. EBM has been acknowledged as a flexible framework for its powerful usage in modeling distribution over highly-structured data, like molecules [25, 32]. To adapt it for MI maximization in our setting, the lower bound can be turned into:

$$\begin{aligned} \mathcal{L}_{\text{Coor-MI}} &= \frac{1}{2} \mathbb{E}_{p(\mathbf{g}_1, \mathbf{g}_2)} \left[\log p(R_1|\mathbf{g}_2) \right] + \frac{1}{2} \mathbb{E}_{p(\mathbf{g}_1, \mathbf{g}_2)} \left[\log p(R_2|\mathbf{g}_1) \right] \\ &= \frac{1}{2} \mathbb{E}_{p(\mathbf{g}_1, \mathbf{g}_2)} \left[\log \frac{\exp(f(R_1, \mathbf{g}_2))}{A_{R_1|\mathbf{g}_2}} \right] + \frac{1}{2} \mathbb{E}_{p(\mathbf{g}_2, \mathbf{g}_1)} \left[\log \frac{\exp(f(R_2, \mathbf{g}_1))}{A_{R_2|\mathbf{g}_1}} \right], \end{aligned} \quad (3)$$

where the $f(\cdot)$ are the negative of energy functions, and $A_{R_1|\mathbf{g}_2}$ and $A_{R_2|\mathbf{g}_1}$ are the intractable partition functions. The first equation in Eq. (3) results from that the two views share the same atom types. This equation can be treated as denoising the atom coordinates of one view from the geometry of the other view. In the following, we will explore how to use the score matching for solving the above EBM, and further transform the coordinate-aware mutual information maximization to the denoising distance matching as the final objective.

4.3 From Coordinate Denoising to Distance Denoising: SE(3)-DDM

Before going into details, first we would like to briefly discuss the denoising score matching (DSM). DSM has three main advantages that inspire us to apply it for solving the coordinate-aware MI. (1) The DSM solution has a nice formulation, such that the final objective function can be simplified

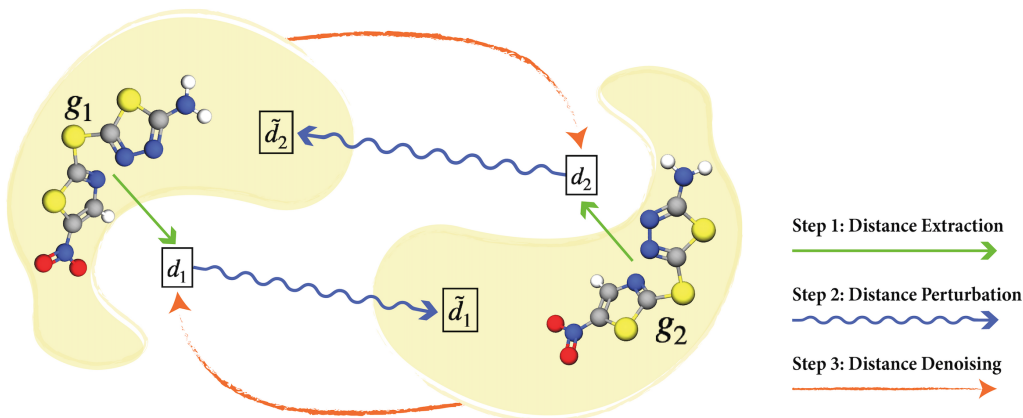


Figure 2: Pipeline for SE(3)-invariant denoising distance matching (SE(3)-DDM). The g_1 and g_2 are around the same local minima, yet with coordinate noises perturbation. Originally we want to do coordinate denoising between these two views. Then as proposed in SE(3)-DDM, we transform it to an equivalent problem, *i.e.*, distance denoising. This figure shows the three key steps: extract the distances from the two geometric views, then perform distance perturbation, and finally denoise the perturbed distances.

with an intuitive explanation: SE(3)-DDM can be seen as solving the denoising pairwise distance at multiple noise levels. (2) The score defined in geometric data can be viewed as a coordinate-based pseudo-force. Such pseudo-force can play an important role for the corresponding geometric representation learning. (3) In terms of the MI maximization, existing methods like InfoNCE [63], EBM-NCE and Representation Reconstruction [34] map the data to the representation space for either inter-data contrastive learning or intra-data reconstruction. This operation can avoid the decoding design issue for highly-structured data [12], yet the trade-off is losing the data-inherent information by certain degree. In other words, the data-level reconstruction task (*e.g.*, DSM) is expected to lead to a more robust representation. Thus, by combining the above three points, we adopt DSM to our problem and propose SE(3)-DDM. We expect that it is able to learn an expressive geometric representation function by solving coordinate-aware SSL task. In addition, the two terms in Eq. (3) are in the mirroring direction. Thus in what follows, we may as well adopt a proxy task that these two directions can be calculated separately, and take one direction for illustration, *e.g.*, $\log \frac{\exp(f(R_1, g_2))}{A_{R_1|g_2}}$.

4.3.1 Denoising Distance Matching

Score. The score is defined as the gradient of the log-likelihood w.r.t. the data, *i.e.*, the atom coordinates in our case. Because the normalization function is a constant w.r.t. the data, it will disappear during the score calculation. To adapt it into our setting, the score is obtained as the gradient of the negative energy function w.r.t. the atom coordinates, as:

$$s(R_1, g_2) \triangleq \nabla_{R_1} \log p(R_1 | g_2) = \nabla_{R_1} f(R_1, g_2). \quad (4)$$

If we assume that the learned optimal energy function, *i.e.*, $f(\cdot)$, possesses certain physical or chemical information, then the score in Eq. (4) can be viewed as a special form of the pseudo-force. This may require more domain-specific knowledge, and we leave this for future exploration.

Score Decomposition: From Coordinates To Distances. Through back-propagation [47], the score on atom coordinates can be further decomposed to the scores attached to pairwise distances:

$$s(R_1, g_2)_i = \sum_{j \neq i} \frac{\partial f(R_1, g_2)}{\partial d_{1,ij}} \cdot \frac{\partial d_{1,ij}}{\partial r_{1,i}} = \sum_{j \neq i} \frac{1}{d_{1,ij}} \cdot s(d_1, g_2)_{ij} \cdot (r_{1,i} - r_{1,j}), \quad (5)$$

where $s(d_1, g_2)_{ij} \triangleq \frac{\partial f(R_1, g_2)}{\partial d_{1,ij}}$. Such decomposition has a nice underlying intuition from the pseudo-force perspective: the pseudo-force on each atom can be further decomposed as the summation of pseudo-forces on the pairwise distances starting from this atom. Note that here the pairwise atoms are connected in the 3D Euclidean space, not by the covalent bonds.

Denoising Distance Matching (DDM). Then we adopt the denoising score matching (DSM) [64] to our task. To be more concrete, we take the Gaussian kernel as the perturbed noise distribution on each pairwise distance, *i.e.*, $q_\sigma(\tilde{d}_1 | g_2) = \mathbb{E}_{p_{\text{data}}(d_1 | g_2)} [q_\sigma(\tilde{d}_1 | d_1)]$, where σ is the deviation in Gaussian

perturbation. One main advantage of using the Gaussian kernel is that the following gradient of conditional log-likelihood has a closed-form formulation: $\nabla_{\tilde{\mathbf{d}}_1} \log q_\sigma(\tilde{\mathbf{d}}_1|\mathbf{d}_1, \mathbf{g}_2) = (\mathbf{d}_1 - \tilde{\mathbf{d}}_1)/\sigma^2$, and the objective function of DSM is to train a score network to match it. This trick was first introduced in [64], and has been widely utilized in the score matching applications [53, 54].

To adapt this into our setting, this is essentially saying that we want to train a “distance network”, *i.e.*, $s_\theta(\tilde{\mathbf{d}}_1|\mathbf{g}_2)$, to match the distance perturbation, or we can say it aims at matching the pseudo-force with the pairwise distances from another aspect. By taking the Fisher divergence as the discrepancy metric and the trick mentioned above, the estimation objective can be simplified to

$$D_F(q_\sigma(\tilde{\mathbf{d}}_1|\mathbf{g}_2)||p_\theta(\tilde{\mathbf{d}}_1|\mathbf{g}_2)) = \frac{1}{2} \mathbb{E}_{p_{\text{data}}(\mathbf{d}_1|\mathbf{g}_2)} \mathbb{E}_{q_\sigma(\tilde{\mathbf{d}}_1|\mathbf{d}_1, \mathbf{g}_2)} \left[\|s_\theta(\tilde{\mathbf{d}}_1, \mathbf{g}_2) - \frac{\mathbf{d}_1 - \tilde{\mathbf{d}}_1}{\sigma^2}\|^2 \right] + C. \quad (6)$$

For more detailed derivations, please refer to Appendix C. In this section, we turn the coordinate-aware MI maximization problem into distance perturbation matching problem, which is equivalent to denoising distance matching. The corresponding pipeline is illustrated in Fig. 2. This can also be explained intuitively. That is, we add the distance noise from \mathbf{d}_1 to $\tilde{\mathbf{d}}_1$ to mimic the coordinate noise between \mathbf{g}_2 and \mathbf{g}_1 , and conduct the denoising distance matching from \mathbf{g}_2 and $\tilde{\mathbf{d}}_1$ to denoise \mathbf{d}_1 .

4.3.2 SE(3)-Invariant Distance Network Modeling

To solve Eq. (6), the key step is to design a SE(3)-invariant distance network. For modeling, we take a SE(3)-equivariant 3D geometric graph neural network as the geometric representation backbone model. Following the notations in Sec. 3 and \mathbf{g}_2 modeling, we can have

$$h(\mathbf{g}_2)_i = \text{3D-GNN}(T(\mathbf{g}_2)), \quad h(\mathbf{g}_2)_{ij} = h(\mathbf{g}_2)_i + h(\mathbf{g}_2)_j, \quad (7)$$

for the atom-level and atom pairwise-level representation respectively. Based on the pairwise representation, we define the distance network as:

$$s_\theta(\tilde{\mathbf{d}}_1, \mathbf{g}_2)_{ij} = \text{MLP}(\text{MLP}(\tilde{\mathbf{d}}_1)_{ij} \oplus h(\mathbf{g}_2)_{ij}). \quad (8)$$

where \oplus is the concatenation and MLP is the multi-layer perceptron. Because the backbone model satisfies SE(3)-equivariance, and our distance network in Eq. (8) is based on a pairwise distance representation and SE(3)-equivariant representation, thus our distance network is SE(3)-invariant.

4.4 Ultimate Training Objective

With the above distance network modeling, we can formulate the ultimate objective function. We adopt the following four model training tricks from [34, 53, 54] to stabilize the score matching training process. (1) We carry out the distance denoising at L -level of noises. (2) We add a weighting coefficient $\lambda(\sigma) = \sigma^\beta$ for each noise level, where β is the annealing factor. (3) We scale the score network by a factor of $1/\sigma$. (4) We sample the exactly same atoms from the two geometry views with masking ratio r . Finally, by considering the two directions and all the above tricks, the objective function for SE(3)-DDM is as follows:

$$\begin{aligned} \mathcal{L}_{\text{SE(3)-DDM}} = & \frac{1}{2L} \sum_{l=1}^L \sigma_l^\beta \mathbb{E}_{p_{\text{data}}(\mathbf{d}_1|\mathbf{g}_2)} \mathbb{E}_{q(\tilde{\mathbf{d}}_1|\mathbf{d}_1, \mathbf{g}_2)} \left[\left\| \frac{s_\theta(\tilde{\mathbf{d}}_1, \mathbf{g}_2)}{\sigma_l} - \frac{\mathbf{d}_1 - \tilde{\mathbf{d}}_1}{\sigma_l^2} \right\|_2^2 \right] \\ & + \frac{1}{2L} \sum_{l=1}^L \sigma_l^\beta \mathbb{E}_{p_{\text{data}}(\mathbf{d}_2|\mathbf{g}_1)} \mathbb{E}_{q(\tilde{\mathbf{d}}_2|\mathbf{d}_2, \mathbf{g}_1)} \left[\left\| \frac{s_\theta(\tilde{\mathbf{d}}_2, \mathbf{g}_1)}{\sigma_l} - \frac{\mathbf{d}_2 - \tilde{\mathbf{d}}_2}{\sigma_l^2} \right\|_2^2 \right]. \end{aligned} \quad (9)$$

The algorithm is in Algorithm 1.

Comparison with score matching in generative modeling. We note that score matching has been widely used for generative modeling task. One of the main drawbacks in the generative setting is the long mixing time for MCMC sampling. However, our work aims at representation learning, so the sampling issue

Algorithm 1 SE(3)-Invariant Denoising Distance Matching

- 1: **Input:** A 3D geometry dataset and L levels of Gaussian noise.
 - 2: **Output:** A pre-trained 3D representation function $h(\cdot)$.
 - 3: **for** each 3D geometry graph \mathbf{g}_1 **do**
 - 4: Obtain its perturbed geometry graph \mathbf{g}_2 .
 - 5: **for** each noise level $l \in \{1, \dots, L\}$ **do**
 - 6: Add noise to the pairwise distance with $\tilde{\mathbf{d}}_1 = \mathbf{d}_1 + \sigma_l$.
 - 7: Add noise to the pairwise distance with $\tilde{\mathbf{d}}_2 = \mathbf{d}_2 + \sigma_l$.
 - 8: Get the score $s_\theta(\tilde{\mathbf{d}}_1, \mathbf{g}_2)$, $s_\theta(\tilde{\mathbf{d}}_2, \mathbf{g}_1)$ with Eq. (8) accordingly.
 - 9: **end for**
 - 10: Update 3D GNN representation function $h(\cdot)$ using Eq. (9).
 - 11: **end for**
-

won’t affect our task. We further note that there also exists a series of work exploring the score matching for conformation generation [47]. However, their scores or pseudo-forces are attached to the 2D topology (the covalent bonds), while our work is based on the pairwise distances from the geometric coordinates only. Merging the heuristic covalent bonds is an interesting future direction.

5 Experiments

In this section, we compare our method with eight pretraining baselines, using 22 downstream tasks including quantum mechanics prediction, force prediction and binding affinity prediction. We compare our method with one randomly-initialized and seven pretraining baselines, which includes six self-supervised learning and one supervised approach, as will be detailed next. We provide all the experiment details (*e.g.*, hyperparameters, dataset specifications) and ablation studies in Appendix D.

5.1 Backbone Models

Our proposed SE(3)-DDM is model-agnostic, and here we evaluate our method using one of the state-of-the-art geometric graph neural networks PaiNN [46]. We also carry out the exactly same experiments on another backbone model (SchNet [44]) in Appendix D.

PaiNN [46] is an improved work of SchNet [44]. It addresses the limitation of rotational equivariance in SchNet by embracing rotational invariance, attaining a more expressive 3D geometric model.

Other backbone models First we want to highlight that what we propose is a general solution and is agnostic to the backbone 3D geometric models. And in addition to the PaiNN, we want to acknowledge that there are more recent progress in this research line, including but not limited to [5, 16, 16, 29, 36, 42, 51]. Yet, they may require large computation resources and may be infeasible (*e.g.*, out of GPU memory) in our setting. The decision is made by considering the model performance, computation efficiency, and memory cost. For more benchmark results and detailed comparisons among 3D geometric models, please check Appendix A.

5.2 Baselines and Pretraining Dataset

Pretraining Dataset The PubChemQC database is a large-scale database with around 4M molecules with 3D geometries, and it calculates both the ground-state and excited-state 3D geometries using DFT (density functional theory). Due to the high computational cost, only several thousand molecules can be processed every day, and this dataset takes years of efforts in total. Following this, Molecule3D [68] takes the ground-state geometries and transforms the data formats into a deep learning-friendly way. It also parses essential quantum properties for each molecule, including energies of the highest occupied molecular orbital (HOMO) and the lowest occupied molecular orbital (LUMO), the energy gap between HOMO-LUMO, and the total energy. For our molecular geometry pretraining, we take 1M molecules from Molecule3D.

Self-Supervised Learning Pretraining Baselines We first consider the following three generative SSL methods: (1) *Type Prediction* is to predict the atom type of masked atoms; (2) *Distance Prediction* aims to predict the pairwise distances among atoms; (3) *Angle Prediction* is to predict the angle among triplet atoms, *i.e.*, the bond angle prediction.

Next, owing to the fact that in Eq. (2) we introduce a coordinate-aware MI maximization objective, we here additionally include two contrastive and one generative SSL baselines. InfoNCE and EBM-NCE [34, 63] are the two widely used contrastive learning loss, where the objective is to simultaneously align the positive views and contrast the negative views. Representation reconstruction (RR) [34] is a generative SSL that is proxy to maximize the MI. It is a more general form of non-contrastive SSL methods including BOYL [21] and SimSiam [8], and the goal is to reconstruct each view from its counterpart in the representation space. Following this, our proposed SE(3)-DDM can be classified as generative SSL, yet it aims at denoising the pairwise distances instead.

Supervised Pretraining Baseline We also compare our method with a supervised pretraining baseline. As aforementioned, the large-scale pretraining dataset uses the DFT to calculate the energy, and extracts the most stable conformers with the lowest energies, which reveal the most fundamental properties of molecules in the 3D Euclidean space. Thus, such energies can be naturally adopted as the supervised signals, and we take this as a supervised pretraining baseline.

Table 1: Downstream results on 12 quantum mechanics prediction tasks from QM9. We take 110K for training, 10K for validation, and 11K for test. The evaluation is mean absolute error, and the best results are in **bold**.

Pretraining	Alpha ↓	Gap ↓	HOMO ↓	LUMO ↓	Mu ↓	Cv ↓	G298 ↓	H298 ↓	R2 ↓	U298 ↓	U0 ↓	Zpve ↓
–	0.048	44.50	26.00	21.11	0.016	0.025	8.31	7.67	0.132	7.77	7.89	1.322
Supervised	0.049	45.33	26.61	21.77	0.016	0.026	8.97	8.59	0.170	8.35	8.19	1.346
Type Prediction	0.050	47.28	30.56	23.18	0.016	0.024	9.32	9.10	0.163	8.94	8.60	1.357
Distance Prediction	0.063	47.62	29.18	22.40	0.019	0.045	12.02	12.31	0.636	11.76	12.22	1.840
Angle Prediction	0.056	47.36	29.53	22.61	0.018	0.027	10.23	10.13	0.143	9.95	9.70	1.643
RR	0.048	44.85	25.42	20.82	0.015	0.025	8.56	8.20	0.133	7.89	7.62	1.329
InfoNCE	0.052	45.65	26.70	21.87	0.016	0.027	9.17	9.62	0.130	8.77	8.63	1.519
EBM-NCE	0.049	44.18	26.29	21.46	0.015	0.026	8.56	8.13	0.126	8.01	7.96	1.447
SE(3)-DDM (ours)	0.046	40.22	23.48	19.42	0.015	0.024	7.65	7.09	0.122	6.99	6.92	1.307

Table 2: Downstream results on 8 force prediction tasks from MD17. We take 1K for training, 1K for validation, and the number of molecules for test are varied among different tasks, ranging from 48K to 991K. The evaluation is mean absolute error, and the best results are in **bold**.

Pretraining	Aspirin ↓	Benzene ↓	Ethanol ↓	Malonaldehyde ↓	Naphthalene ↓	Salicylic ↓	Toluene ↓	Uracil ↓
–	0.556	0.052	0.213	0.338	0.138	0.288	0.155	0.194
Supervised	0.478	0.145	0.318	0.434	0.460	0.527	0.251	0.404
Type Prediction	1.656	0.349	0.414	0.886	1.684	1.807	0.660	1.020
Distance Prediction	1.434	0.090	0.378	1.017	0.631	1.569	0.350	0.415
Angle Prediction	0.839	0.105	0.337	0.517	0.772	0.931	0.274	0.676
RR	0.502	0.052	0.219	0.334	0.130	0.312	0.152	0.192
InfoNCE	0.881	0.066	0.275	0.550	0.356	0.607	0.186	0.559
EBM-NCE	0.598	0.073	0.237	0.518	0.246	0.416	0.178	0.475
SE(3)-DDM (ours)	0.453	0.051	0.166	0.288	0.129	0.266	0.122	0.183

5.3 Downstream Tasks on Quantum Mechanics and Force Prediction

QM9 [41] is a dataset of 134K molecules consisting of 9 heavy atoms. It includes 12 tasks that are related to the quantum properties. For example, U0 and U298 are the internal energies at 0K at 0K and 298.15K respectively, and U298 and G298 are the other two energies that can be transferred from H298 respectively. The other 8 tasks are quantum mechanics related to the DFT process. MD17 [9] is a dataset on molecular dynamics simulation. It includes eight tasks, corresponding to eight organic molecules, and each task includes the molecule positions along the potential energy surface (PES), as shown in Fig. 1. The goal is to predict the energy-conserving interatomic forces for each atom in each molecule position. We follow the literature [30, 36, 45, 46] of using 1K for training and 1K for validation, while the test set (from 48K to 991K) is much larger.

The results on QM9 and MD17 are displayed in Tables 1 and 2 respectively. From Tables 1 and 2, we can observe that most the pretraining baselines tested perform on par with or even worse than the randomly-initialized baseline. The top performing baseline is the representation reconstruction method (RR), which optimizes the coordinate-aware MI; it outperforms the other baselines on 5 out of 12 tasks in QM9 and 6 out of 8 tasks in MD17. This implies the potential of applying generative SSL for maximizing this coordinate-aware MI. Promisingly, our proposed SE(3)-DDM achieves consistently improved performance on all the 20 tasks in QM9 and MD17. All these observations empirically verify the effectiveness of the distance denoising, which models the most determinant factor in molecule geometric data.

5.4 Downstream Tasks on Binding Affinity Prediction

Atom3D [61] is a recently published dataset. It gathers several core tasks for 3D molecules, including binding affinity. The binding affinity prediction is to measure the strength of binding interaction between a small molecule to the target protein. Here we will model both the small molecule and protein with their 3D atom coordinates provided. We follow Atom3D in data preprocessing and data splitting. For more detailed discussions and statistics, please check Appendix D.

During the binding process, there is a cavity in a protein that can potentially possess suitable properties for binding a small molecule (ligand), and it is termed a pocket [57]. Because of the large volume of protein, we follow [61] by only taking the binding pocket, where there are no more than 600 atoms for each molecule and protein pair. To be more concrete, we consider two binding affinity tasks. (1) The first task is ligand binding affinity (LBA). It is gathered from [65] and the task is to predict the binding affinity strength between a small molecule and a protein pocket. (2) The second task is ligand efficacy prediction (LEP). The input is a ligand and both the active and inactive conformers of a protein, and the goal is to predict whether or not the ligand can activate the protein’s function.

Table 3: Downstream results on 2 binding affinity prediction tasks. We select three evaluation metrics for LBA: the root mean squared error (RMSD), the Pearson correlation (R_P) and the Spearman correlation (R_S). LEP is a binary classification task, and we use the area under the curve for receiver operating characteristics (ROC) and precision-recall (PR) for evaluation. We run cross validation with 5 seeds, and the best results are in **bold**.

Pretraining	LBA			LEP	
	RMSD \downarrow	R_P \uparrow	R_C \uparrow	ROC \uparrow	PR \uparrow
–	1.463 \pm 0.06	0.572 \pm 0.02	0.568 \pm 0.02	0.675 \pm 0.04	0.549 \pm 0.05
Supervised	1.551 \pm 0.08	0.539 \pm 0.03	0.533 \pm 0.03	0.696 \pm 0.03	0.554 \pm 0.03
Charge Prediction	2.316 \pm 0.80	0.387 \pm 0.11	0.400 \pm 0.11	0.630 \pm 0.05	0.557 \pm 0.07
Distance Prediction	1.542 \pm 0.08	0.545 \pm 0.03	0.540 \pm 0.03	0.521 \pm 0.07	0.479 \pm 0.07
Angle Prediction	–	–	–	0.545 \pm 0.07	0.504 \pm 0.07
RR	1.515 \pm 0.07	0.545 \pm 0.03	0.539 \pm 0.03	0.654 \pm 0.05	0.518 \pm 0.06
InfoNCE	1.564 \pm 0.05	0.508 \pm 0.03	0.497 \pm 0.05	0.693 \pm 0.06	0.571 \pm 0.08
EBM-NCE	1.499 \pm 0.06	0.547 \pm 0.03	0.534 \pm 0.03	0.691 \pm 0.05	0.603 \pm 0.07
SE(3)-DDM (ours)	1.451 \pm 0.03	0.577 \pm 0.02	0.572 \pm 0.01	0.776 \pm 0.03	0.694 \pm 0.06

Results in Table 3 indicate that, for the LBA task, one pretraining method fails to generalize to LBA (the loss gets too large), and all the other pretraining baselines cannot beat the randomly-initialized baseline. For the LEP task, the supervised and two contrastive learning pretraining baselines stand out for both ROC and PR metrics. Meaningfully, for both tasks, SE(3)-DDM is able to achieve promising improvement, revealing that modeling the local region around conformer with distance denoising can also benefit for binding affinity downstream tasks.

5.5 Discussion: Connection with Multi-task Pretraining

In the above experiments, we test multiple self-supervised and supervised pretraining tasks separately. Yet, all these pretraining methods are not contradict, but could be complementary instead. Existing work has successfully shown the effect of combining them in various ways. For example, [26] shows that jointly doing supervised and self-supervised pretraining can augment the pretrained representation. [34, 52] prove that contrastive and generative SSL pretraining methods can be learned simultaneously as a multi-task pretraining. In addition, in terms of the molecule-specific pretraining, [34] empirically verifies that 2D topology and 3D geometry views can share certain information, and maximizing their mutual information together with topology SSL for pretraining is beneficial.

With these insights, we would like to claim that all of these points are worth exploration in the future, especially in the line of pretraining for molecular geometry. Because pretraining datasets often come with multiple quantum properties and the 2D molecular topology can be obtained heuristically. Yet as the first step to explore the self-supervised learning using only the 3D geometric data (*i.e.*, without covalent bonds), our study here would like to leave multi-task pretraining for future exploration.

6 Conclusions and Future Directions

We proposed a novel coordinate denoising method, coined SE(3)-DDM, for molecular geometry pretraining. SE(3)-DDM leverages a SE(3)-invariant score matching strategy to successfully decompose its coordinate denoising objective into the denoising of pairwise atomic distances in a molecule, which then can be effectively computed and directly target the determinant factors in geometric data. We empirically verified the effectiveness and robustness of our method, outperforming 8 state-of-the-art pretraining baselines on 22 benchmarking geometric molecular prediction tasks.

Our work opens venues from multiple promising directions. First from the machine learning perspective, we propose a general pipeline on using Energy Based Model (EBM) for MI maximization. Yet, there are more explorations on the success of EBM, like GFlowNet [3], and it would be interesting to explore how to combine it with molecular geometric data along this systematic path. In addition, SE(3)-DDM does not utilize the 2D structure (*i.e.*, covalent bonds for molecules), and it would be desirable to consider how to utilize the distance denoising together with the 2D topology information.

In terms of applications, our proposed SE(3)-DDM is a general framework, and it can be naturally applied to other geometric data, such as point cloud and protein pretraining. In addition, our current goal is to perform denoising in the local region, yet it would be interesting to explore larger regions. From this aspect, the denoising can be viewed as recovering the molecular dynamics trajectory, and we would explore how generalizable this pretrained representation is to the downstream tasks.

Acknowledgement

We would like to thank Anima Anandkumar, Chaowei Xiao, Weili Nie, Zhuoran Qiao, and Chengpeng Wang for insightful discussions. This project is supported by the Natural Sciences and Engineering Research Council (NSERC) Discovery Grant, the Canada CIFAR AI Chair Program, collaboration grants between Microsoft Research and Mila, Samsung Electronics Co., Ltd., Amazon Faculty Research Award, Tencent AI Lab Rhino-Bird Gift Fund and two NRC Collaborative R&D Projects (AI4D-CORE-06, AI4D-CORE-08). This project was also partially funded by IVADO Fundamental Research Project grant PRF-2019-3583139727.

References

- [1] Kenneth Atz, Francesca Grisoni, and Gisbert Schneider. Geometric deep learning on molecular representations. *Nature Machine Intelligence*, pages 1–10, 2021. 2
- [2] Simon Axelrod and Rafael Gomez-Bombarelli. Geom: Energy-annotated molecular conformations for property prediction and molecular generation. *arXiv preprint arXiv:2006.05531*, 2020. 3
- [3] Yoshua Bengio, Tristan Deleu, Edward J Hu, Salem Lahlou, Mo Tiwari, and Emmanuel Bengio. Gflownet foundations. *arXiv preprint arXiv:2111.09266*, 2021. 9
- [4] Avrim Blum and Tom Mitchell. Combining labeled and unlabeled data with co-training. In *Proceedings of the eleventh annual conference on Computational learning theory*, pages 92–100, 1998. 19
- [5] Johannes Brandstetter, Rob Hesselink, Elise van der Pol, Erik Bekkers, and Max Welling. Geometric and physical quantities improve e(3) equivariant message passing. *arXiv preprint arXiv:2110.02905*, 2021. 2, 7, 14
- [6] Nathan Brown, Marco Fiscato, Marwin HS Segler, and Alain C Vaucher. Guacamol: benchmarking models for de novo molecular design. *Journal of chemical information and modeling*, 59(3):1096–1108, 2019. 1
- [7] Jintai Chen, Biwen Lei, Qingyu Song, Haochao Ying, Danny Z Chen, and Jian Wu. A hierarchical graph network for 3d object detection on point clouds. In *Proceedings of the IEEE/CVF conference on computer vision and pattern recognition*, pages 392–401, 2020. 2
- [8] Xinlei Chen and Kaiming He. Exploring simple siamese representation learning. In *Proceedings of the IEEE/CVF Conference on Computer Vision and Pattern Recognition*, pages 15750–15758, 2021. 7
- [9] Stefan Chmiela, Alexandre Tkatchenko, Huziel E Sauceda, Igor Poltavsky, Kristof T Schütt, and Klaus-Robert Müller. Machine learning of accurate energy-conserving molecular force fields. *Science advances*, 3(5):e1603015, 2017. 8, 20
- [10] John D Chodera and Frank Noé. Markov state models of biomolecular conformational dynamics. *Current opinion in structural biology*, 25:135–144, 2014. 2, 16
- [11] Yilun Du, Shuang Li, Joshua Tenenbaum, and Igor Mordatch. Improved contrastive divergence training of energy based models. *arXiv preprint arXiv:2012.01316*, 2020. 3
- [12] Yuanqi Du, Tianfan Fu, Jimeng Sun, and Shengchao Liu. Molgensurvey: A systematic survey in machine learning models for molecule design. *arXiv preprint arXiv:2203.14500*, 2022. 5
- [13] David Duvenaud, Dougal Maclaurin, Jorge Aguilera-Iparraguirre, Rafael Gómez-Bombarelli, Timothy Hirzel, Alán Aspuru-Guzik, and Ryan P Adams. Convolutional networks on graphs for learning molecular fingerprints. *arXiv preprint arXiv:1509.09292*, 2015. 1
- [14] Thomas Engel and Johann Gasteiger. *Applied chemoinformatics: achievements and future opportunities*. John Wiley & Sons, 2018. 15
- [15] Xiaomin Fang, Lihang Liu, Jieqiong Lei, Donglong He, Shanzhuo Zhang, Jingbo Zhou, Fan Wang, Hua Wu, and Haifeng Wang. Chemrl-gem: Geometry enhanced molecular representation learning for property prediction. *arXiv preprint arXiv:2106.06130*, 2021. 3
- [16] Fabian B Fuchs, Daniel E Worrall, Volker Fischer, and Max Welling. Se(3)-transformers: 3d roto-translation equivariant attention networks. *arXiv preprint arXiv:2006.10503*, 2020. 2, 7, 14
- [17] Siddhant Garg and Yingyu Liang. Functional regularization for representation learning: A unified theoretical perspective. *Advances in Neural Information Processing Systems*, 33:17187–17199, 2020. 19

- [18] Justin Gilmer, Samuel S Schoenholz, Patrick F Riley, Oriol Vinyals, and George E Dahl. Neural message passing for quantum chemistry. In *International conference on machine learning*, pages 1263–1272. PMLR, 2017. 1
- [19] Jonathan Godwin, Michael Schaarschmidt, Alexander L Gaunt, Alvaro Sanchez-Gonzalez, Yulia Rubanova, Petar Veličković, James Kirkpatrick, and Peter Battaglia. Simple GNN regularisation for 3d molecular property prediction and beyond. In *International Conference on Learning Representations*, 2022. 16
- [20] Sai Krishna Gottipati, Boris Sattarov, Sufeng Niu, Yashaswi Pathak, Haoran Wei, Shengchao Liu, Simon Blackburn, Karam Thomas, Connor Coley, Jian Tang, et al. Learning to navigate the synthetically accessible chemical space using reinforcement learning. In *International Conference on Machine Learning*, pages 3668–3679. PMLR, 2020. 1
- [21] Jean-Bastien Grill, Florian Strub, Florent Altché, Corentin Tallec, Pierre Richemond, Elena Buchatskaya, Carl Doersch, Bernardo Avila Pires, Zhaohan Guo, Mohammad Gheshlaghi Azar, et al. Bootstrap your own latent-a new approach to self-supervised learning. *Advances in Neural Information Processing Systems*, 33:21271–21284, 2020. 7
- [22] Yuzhi Guo, Jiaxiang Wu, Hehuan Ma, and Junzhou Huang. Self-supervised pre-training for protein embeddings using tertiary structures. 2022. 14
- [23] Michael Gutmann and Aapo Hyvärinen. Noise-contrastive estimation: A new estimation principle for unnormalized statistical models. In *Proceedings of the thirteenth international conference on artificial intelligence and statistics*, pages 297–304. JMLR Workshop and Conference Proceedings, 2010. 3, 16, 17, 18
- [24] Thomas A Halgren. Merck molecular force field. i. basis, form, scope, parameterization, and performance of mmff94. *Journal of computational chemistry*, 17(5-6):490–519, 1996. 15
- [25] Ryuichiro Hataya, Hideki Nakayama, and Kazuki Yoshizoe. Graph energy-based model for molecular graph generation. In *Energy Based Models Workshop-ICLR 2021*, 2021. 4
- [26] Weihua Hu, Bowen Liu, Joseph Gomes, Marinka Zitnik, Percy Liang, Vijay Pande, and Jure Leskovec. Strategies for pre-training graph neural networks. In *International Conference on Learning Representations, ICLR*, 2020. 1, 3, 9
- [27] Ziniu Hu, Yuxiao Dong, Kuansan Wang, Kai-Wei Chang, and Yizhou Sun. Gpt-gnn: Generative pre-training of graph neural networks. In *ACM SIGKDD International Conference on Knowledge Discovery & Data Mining, KDD*, pages 1857–1867, 2020. 3
- [28] Aapo Hyvärinen and Peter Dayan. Estimation of non-normalized statistical models by score matching. *Journal of Machine Learning Research*, 6(4), 2005. 3
- [29] Johannes Klicpera, Florian Becker, and Stephan Günnemann. Gemnet: Universal directional graph neural networks for molecules. In *Conference on Neural Information Processing Systems (NeurIPS)*, 2021. 2, 7, 14
- [30] Johannes Klicpera, Shankari Giri, Johannes T Margraf, and Stephan Günnemann. Fast and uncertainty-aware directional message passing for non-equilibrium molecules. *arXiv preprint arXiv:2011.14115*, 2020. 2, 8, 14
- [31] Greg Landrum et al. RDKit: A software suite for cheminformatics, computational chemistry, and predictive modeling, 2013. 15
- [32] Meng Liu, Keqiang Yan, Bora Oztekin, and Shuiwang Ji. Graphebm: Molecular graph generation with energy-based models. *arXiv preprint arXiv:2102.00546*, 2021. 4
- [33] Shengchao Liu, Mehmet Furkan Demirel, and Yingyu Liang. N-gram graph: Simple unsupervised representation for graphs, with applications to molecules. *arXiv preprint arXiv:1806.09206*, 2018. 1, 3
- [34] Shengchao Liu, Hanchen Wang, Weiyang Liu, Joan Lasenby, Hongyu Guo, and Jian Tang. Pre-training molecular graph representation with 3d geometry. In *International Conference on Learning Representations*, 2022. 1, 3, 5, 6, 7, 9, 18, 19
- [35] Xiao Liu, Fanjin Zhang, Zhenyu Hou, Li Mian, Zhaoyu Wang, Jing Zhang, and Jie Tang. Self-supervised learning: Generative or contrastive. *IEEE Transactions on Knowledge and Data Engineering*, 2021. 3
- [36] Yi Liu, Limei Wang, Meng Liu, Xuan Zhang, Bora Oztekin, and Shuiwang Ji. Spherical message passing for 3d graph networks. *arXiv preprint arXiv:2102.05013*, 2021. 2, 7, 8, 14, 20

- [37] Yixin Liu, Shirui Pan, Ming Jin, Chuan Zhou, Feng Xia, and Philip S Yu. Graph self-supervised learning: A survey. *arXiv preprint arXiv:2103.00111*, 2021. 3
- [38] Ilya Loshchilov and Frank Hutter. Sgdr: Stochastic gradient descent with warm restarts. *arXiv preprint arXiv:1608.03983*, 2016. 14, 21
- [39] Francesca Pistilli, Giulia Fracastoro, Diego Valsesia, and Enrico Magli. Learning graph-convolutional representations for point cloud denoising. In *European conference on computer vision*, pages 103–118. Springer, 2020. 2
- [40] Charles Ruizhongtai Qi, Li Yi, Hao Su, and Leonidas J Guibas. Pointnet++: Deep hierarchical feature learning on point sets in a metric space. *Advances in neural information processing systems*, 30, 2017. 2
- [41] Raghunathan Ramakrishnan, Pavlo O Dral, Matthias Rupp, and O Anatole Von Lilienfeld. Quantum chemistry structures and properties of 134 kilo molecules. *Scientific data*, 1(1):1–7, 2014. 8, 20
- [42] Victor Garcia Satorras, Emiel Hoogetboom, and Max Welling. E(n) equivariant graph neural networks. *arXiv preprint arXiv:2102.09844*, 2021. 2, 7, 14
- [43] H Bernhard Schlegel. Exploring potential energy surfaces for chemical reactions: an overview of some practical methods. *Journal of computational chemistry*, 24(12):1514–1527, 2003. 2
- [44] Kristof T Schütt, Pieter-Jan Kindermans, Huziel E Sauceda, Stefan Chmiela, Alexandre Tkatchenko, and Klaus-Robert Müller. Schnet: A continuous-filter convolutional neural network for modeling quantum interactions. *arXiv preprint arXiv:1706.08566*, 2017. 7, 14
- [45] Kristof T Schütt, Huziel E Sauceda, P-J Kindermans, Alexandre Tkatchenko, and K-R Müller. Schnet—a deep learning architecture for molecules and materials. *The Journal of Chemical Physics*, 148(24):241722, 2018. 2, 8, 14, 20
- [46] Kristof T Schütt, Oliver T Unke, and Michael Gastegger. Equivariant message passing for the prediction of tensorial properties and molecular spectra. *arXiv preprint arXiv:2102.03150*, 2021. 2, 7, 8, 14, 20
- [47] Chence Shi, Shitong Luo, Minkai Xu, and Jian Tang. Learning gradient fields for molecular conformation generation. In *International Conference on Machine Learning*, pages 9558–9568. PMLR, 2021. 5, 7, 18
- [48] Chence Shi, Minkai Xu, Hongyu Guo, Ming Zhang, and Jian Tang. A graph to graphs framework for retrosynthesis prediction. In *International Conference on Machine Learning*, pages 8818–8827. PMLR, 2020. 1
- [49] Chence Shi, Minkai Xu, Zhaocheng Zhu, Weinan Zhang, Ming Zhang, and Jian Tang. Graphaf: a flow-based autoregressive model for molecular graph generation. *arXiv preprint arXiv:2001.09382*, 2020. 1
- [50] Weijing Shi and Raj Rajkumar. Point-gnn: Graph neural network for 3d object detection in a point cloud. In *Proceedings of the IEEE/CVF conference on computer vision and pattern recognition*, pages 1711–1719, 2020. 2
- [51] Muhammed Shuaibi, Adeesh Kolluru, Abhishek Das, Aditya Grover, Anuroop Sriram, Zachary Ulissi, and C Lawrence Zitnick. Rotation invariant graph neural networks using spin convolutions. *arXiv preprint arXiv:2106.09575*, 2021. 2, 7, 14
- [52] Gowthami Somepalli, Micah Goldblum, Avi Schwarzschild, C Bayan Bruss, and Tom Goldstein. Saint: Improved neural networks for tabular data via row attention and contrastive pre-training. *arXiv preprint arXiv:2106.01342*, 2021. 9
- [53] Yang Song and Stefano Ermon. Generative modeling by estimating gradients of the data distribution. *Advances in Neural Information Processing Systems*, 32, 2019. 6, 18
- [54] Yang Song and Stefano Ermon. Improved techniques for training score-based generative models. *Advances in neural information processing systems*, 33:12438–12448, 2020. 6, 18
- [55] Yang Song and Diederik P Kingma. How to train your energy-based models. *arXiv preprint arXiv:2101.03288*, 2021. 3, 16
- [56] Yang Song, Jascha Sohl-Dickstein, Diederik P Kingma, Abhishek Kumar, Stefano Ermon, and Ben Poole. Score-based generative modeling through stochastic differential equations. *arXiv preprint arXiv:2011.13456*, 2020. 3, 16, 18

- [57] Antonia Stank, Daria B Kokh, Jonathan C Fuller, and Rebecca C Wade. Protein binding pocket dynamics. *Accounts of chemical research*, 49(5):809–815, 2016. 8, 20
- [58] Fan-Yun Sun, Jordan Hoffmann, Vikas Verma, and Jian Tang. Infograph: Unsupervised and semi-supervised graph-level representation learning via mutual information maximization. In *International Conference on Learning Representations, ICLR*, 2020. 1, 3
- [59] Ruoxi Sun, Hanjun Dai, Li Li, Steven Kearnes, and Bo Dai. Energy-based view of retrosynthesis. *arXiv preprint arXiv:2007.13437*, 2020. 1
- [60] Nathaniel Thomas, Tess Smidt, Steven Kearnes, Lusann Yang, Li Li, Kai Kohlhoff, and Patrick Riley. Tensor field networks: Rotation-and translation-equivariant neural networks for 3d point clouds. *arXiv preprint arXiv:1802.08219*, 2018. 2
- [61] Raphael JL Townshend, Martin Vögele, Patricia Suriana, Alexander Derry, Alexander Powers, Yianni Laloudakis, Sidhika Balachandar, Brandon Anderson, Stephan Eismann, Risi Kondor, et al. Atom3d: Tasks on molecules in three dimensions. *arXiv preprint arXiv:2012.04035*, 2020. 8, 20
- [62] Mikaela Angelina Uy, Quang-Hieu Pham, Binh-Son Hua, Thanh Nguyen, and Sai-Kit Yeung. Revisiting point cloud classification: A new benchmark dataset and classification model on real-world data. In *Proceedings of the IEEE/CVF international conference on computer vision*, pages 1588–1597, 2019. 2
- [63] Aaron Van den Oord, Yazhe Li, and Oriol Vinyals. Representation learning with contrastive predictive coding. *arXiv e-prints*, pages arXiv–1807, 2018. 5, 7
- [64] Pascal Vincent. A connection between score matching and denoising autoencoders. *Neural computation*, 23(7):1661–1674, 2011. 3, 5, 6, 18
- [65] Renxiao Wang, Xueliang Fang, Yipin Lu, Chao-Yie Yang, and Shaomeng Wang. The pdbbind database: methodologies and updates. *Journal of medicinal chemistry*, 48(12):4111–4119, 2005. 8, 21
- [66] Lirong Wu, Haitao Lin, Zhangyang Gao, Cheng Tan, Stan Li, et al. Self-supervised on graphs: Contrastive, generative, or predictive. *arXiv preprint arXiv:2105.07342*, 2021. 3
- [67] Yaochen Xie, Zhao Xu, Jingtun Zhang, Zhengyang Wang, and Shuiwang Ji. Self-supervised learning of graph neural networks: A unified review. *arXiv preprint arXiv:2102.10757*, 2021. 3
- [68] Zhao Xu, Youzhi Luo, Xuan Zhang, Xinyi Xu, Yaochen Xie, Meng Liu, Kaleb Dickerson, Cheng Deng, Maho Nakata, and Shuiwang Ji. Molecule3d: A benchmark for predicting 3d geometries from molecular graphs. *arXiv preprint arXiv:2110.01717*, 2021. 7
- [69] Kevin Yang, Kyle Swanson, Wengong Jin, Connor Coley, Philipp Eiden, Hua Gao, Angel Guzman-Perez, Timothy Hopper, Brian Kelley, Miriam Mathea, et al. Analyzing learned molecular representations for property prediction. *Journal of chemical information and modeling*, 59(8):3370–3388, 2019. 1
- [70] Yuning You, Tianlong Chen, Yongduo Sui, Ting Chen, Zhangyang Wang, and Yang Shen. Graph contrastive learning with augmentations. In *Advances in Neural Information Processing Systems, NeurIPS*, 2020. 1, 3
- [71] Chengxi Zang and Fei Wang. Moflow: an invertible flow model for generating molecular graphs. In *Proceedings of the 26th ACM SIGKDD International Conference on Knowledge Discovery & Data Mining*, pages 617–626, 2020. 1

A Benchmarks and Related Work

A.1 Geometric Neural Networks

Recently, geometric neural networks have been actively proposed, including SchNet [45], TFN [16], DimeNet++ [30], SE(3)-Trans [16], EGNN [42], SEGNN [5], SphereNet [36], SpinConv [51], PaiNN [46], and GemNet [29]. We reproduce most of them on the QM9 dataset as shown in Table 4. Among this, we would like to highlight two models: SchNet and PaiNN.

SchNet [44] is composed of the following key steps:

$$z_i^{(0)} = \text{embedding}(x_i), \quad z_i^{(t+1)} = \text{MLP}\left(\sum_{j=1}^n f(x_j^{(t-1)}, r_i, r_j)\right), \quad h_i = \text{MLP}(z_i^{(K)}), \quad (10)$$

where K is the number of hidden layers, and

$$f(x_j, r_i, r_j) = x_j \cdot e_k(r_i - r_j) = x_j \cdot \exp(-\gamma \| \|r_i - r_j\|_2 - \mu \|_2^2) \quad (11)$$

is the continuous-filter convolution layer, enabling the modeling of continuous coordinates of atoms.

PaiNN [46] is an improved work of SchNet [44]. It addresses the limitation of rotational equivariance in SchNet by embracing rotational invariance, attaining a more expressive 3D geometric model.

A.2 Benchmark on QM9

Current work is using different optimization strategies and different data split (in terms of the splitting size). Originally there are 133,885 molecules in QM9, where 3,054 are filtered out, leading to 130,831 molecules. During the benchmark, we find that:

- The performance on QM9 is very robust to either using (1) 110K for training, 10K for val, 10,831 for test or using (2) 100K for training, 13,083 for val and 17,748 for test.
- The optimization, especially the learning rate scheduler is very critical. During the benchmarking, we find that using cosine annealing learning rate schedule [38] is generally the most robust.

For more detailed discussion on QM9, please refer to Appendix D. We show the benchmark results on QM9 in Table 4.

Table 4: Benchmark results on 12 quantum mechanics prediction tasks from QM9. We take 110K for training, 10K for validation, and 11K for test. The evaluation is mean absolute error (MAE).

	Alpha ↓	Gap ↓	HOMO ↓	LUMO ↓	Mu ↓	Cv ↓	G298 ↓	H298 ↓	R2 ↓	U298 ↓	U0 ↓	Zpve ↓
SchNet	0.070	50.38	31.81	25.76	0.029	0.031	14.60	14.24	0.131	13.99	14.12	1.686
SE(3)-Trans	0.136	58.27	35.95	35.41	0.052	0.068	68.50	70.22	1.828	70.14	72.28	5.302
EGNN	0.067	48.77	28.98	24.44	0.032	0.031	11.02	11.07	0.078	10.83	10.70	1.578
DimeNet++	0.046	38.14	21.23	17.57	0.029	0.022	7.98	7.19	0.306	6.86	6.93	1.204
SphereNet	0.050	39.54	21.88	18.66	0.026	0.025	8.65	7.43	0.262	8.28	8.01	1.390
SEGNN	0.057	41.08	22.46	21.46	0.025	0.028	13.07	13.94	0.472	14.64	13.89	1.662
PaiNN	0.048	44.50	26.00	21.11	0.016	0.025	8.31	7.67	0.132	7.77	7.89	1.322

A.3 Related Work

We acknowledge that there is a parallel work called Protein Tertiary SSL (PTSSL) [22] working on the geometric self-supervised learning. Yet, there are some fundamental differences between theirs and ours, as listed below: **(1) Key notion on pseudo-force.** PTSSL directly applies the denoised score matching method into protein tertiary structures, yet our focus is on how the notion of pseudo-force can come into the play, which possess better generalization ability. **(2) Task setting.** PTSSL works on protein and utilize both the 2D and 3D information, and our work is purely working on the 3D geometric information. **(3) Technical novelty.** PTSSL designs the DSM objective for SSL, and what we propose is a systematic tool: using energy-based model and score matching to solve the geometric SSL problem opens a new venue in this field. **(4) Objective.** PTSSL directly designs one objective function, which is denoising from one view to the other. Ours starts from the lower bound of MI, which is symmetric in terms of the denoising directions. We believe that such symmetry are treating the two views equally, and can better reveal the mutual concept, making the pre-trained representation more robust to the position augmentations. **(5) Empirical baseline.** PTSSL lacks the comparisons with other pre-training methods, while we compare with 7 SOTA pre-training methods, especially those driven by maximizing the MI with the same augmentations. Without such comparisons, it is hard to tell the effectiveness of the pseudo-force matching for geometric data. **(6) Score network.** Last but not least, the score network designed in PTSSL does not satisfy the SE(3) equivariant property.

B An Example On The Importance of Atom Coordinates

First it has been widely acknowledged [14] that the atom positions or molecule shapes are important factors to the quantum properties. Here we carry out an evidence example to empirically verify this. The goal here is to make predictions on 12 quantum properties in QM9.

The molecule geometric data includes two main components as input features: the atom types and atom coordinates. Other key information can be inferred accordingly, including the pairwise distances and torsion angles. We consider corruption on each of the component to empirically test their importance accordingly.

- Atom type corruption. There are in total 118 types of atom types, and the standard embedding option is to apply the one-hot encoding. In the corruption case, we replace all the atom types with a hold-out index, *i.e.*, index 119.
- Atom coordinate corruption. Originally QM9 includes atom coordinates that are in the stable state, and now we replace them with the coordinates generated with MMFF [24] from RDKit [31].

Table 5: An evidence example on molecular data. The goal is to predict 12 quantum properties (regression tasks) of 3D molecules (with 3D coordinates on each atom). The evaluation metric is MAE.

Model	Mode	Alpha ↓	Gap ↓	HOMO ↓	LUMO ↓	Mu ↓	Cv ↓	G298 ↓	H298 ↓	R2 ↓	U298 ↓	U0 ↓	Zpve ↓
SchNet	Stable Geometry	0.070	50.59	32.53	26.33	0.029	0.032	14.68	14.85	0.122	14.70	14.44	1.698
	Type Corruption	0.074	52.07	33.64	26.75	0.032	0.032	21.68	22.93	0.231	23.01	22.99	1.677
	Coordinate Corruption	0.265	110.59	79.92	78.59	0.422	0.113	57.07	58.92	18.649	60.71	59.32	5.151
PaiNN	Stable Geometry	0.048	44.50	26.00	21.11	0.016	0.025	8.31	7.67	0.132	7.77	7.89	1.322
	Type Corruption	0.057	45.61	27.22	22.16	0.016	0.025	11.48	11.60	0.181	11.15	10.89	1.339
	Coordinate Corruption	0.223	108.31	73.43	72.35	0.391	0.095	48.40	51.82	16.828	51.43	48.95	4.395

We take SchNet and PaiNN as the backbone 3D GNN models, and the results are in Table 5. We can observe that (1) Both corruption examples lead to performance decrease. (2) The atom coordinate corruption may lead to more severe performance decrease than the atom type corruption. To put this into another way is that, when we corrupt the atom types with the same hold-out type, it is equivalently to removing the atom type information. Thus, this can be viewed as using the equilibrium atom coordinates alone, and the property prediction is comparatively robust. This observation can also be supported from the domain perspective. According to the valence bond theory, the atom type information can be implicitly and roughly inferred from the atom coordinates.

Therefore, by combining all the above observations and analysis, one can draw the conclusion that, *for molecule geometry data, the atom coordinates reveal more fundamental information for representation learning.*

C Mutual Information Maximization with Energy-Based Model

In this section, we will give a detailed discussion on the mutual information (MI) maximization with energy-based model (EBM).

First, let us recall the definition of MI. MI measures the non-linear dependency between two variables, defined as:

$$I(\mathbf{g}_1; \mathbf{g}_2) = \mathbb{E}_{p(\mathbf{g}_1, \mathbf{g}_2)} \left[\log \frac{p(\mathbf{g}_1, \mathbf{g}_2)}{p(\mathbf{g}_1)p(\mathbf{g}_2)} \right]. \quad (12)$$

Notice that to keep consistent with the notations above, we will be using \mathbf{g}_1 and \mathbf{g}_2 as the two variables. Then we can obtain a lower bound to MI:

$$I(\mathbf{g}_1; \mathbf{g}_2) = \mathbb{E}_{p(\mathbf{g}_1, \mathbf{g}_2)} \left[\log \frac{p(\mathbf{g}_1, \mathbf{g}_2)}{p(\mathbf{g}_1)p(\mathbf{g}_2)} \right] \geq \frac{1}{2} \mathbb{E}_{p(\mathbf{g}_1, \mathbf{g}_2)} \left[\log p(\mathbf{g}_1 | \mathbf{g}_2) + \log p(\mathbf{g}_2 | \mathbf{g}_1) \right] \triangleq \mathcal{L}_{\text{MI}}. \quad (13)$$

Thus, we transform the MI maximization problem into maximizing the summation of two conditional log-likelihoods. Such objective function opens a wider venue for estimating MI, *e.g.*, using the EBM to estimate Eq. (13).

Adaptation to Geometric Data The 3D geometric information, or the atomic coordinates are critical to molecular properties. Then based on this, we propose a geometry perturbation, which adds small noises to the atom coordinates. This geometry perturbation possess certain motivations from both domain and machine learning perspectives. (1) From the practical experiment perspective, the statistical and systematic errors [10] on conformation estimation are unavoidable. Coordinate perturbation is a natural way to enable learning representations robust to such noises. (2) From the domain aspect, molecules are not static but in a continuous motion in the 3D Euclidean space, and we can obtain a potential energy surface accordingly. We are interested in modeling the conformer, *i.e.*, the 3D coordinates with the lowest energy. However, even the conformer at the lowest energy point can have vibrations, and coordinate perturbation can better capture such movement yet with the same order of magnitude on energies. (3) As will be illustrated later, our proposed method can be simplified as denoising atomic distance matching. (4) Leveraging coordinate perturbation for model regularization has also been empirically verified its effectiveness for supervised molecule geometric representation learning [19]. Such characteristics of the molecular geometry motivate us to apply the coordinate perturbation. If we take each of the two views as adding noise to the coordinates from the other view, then the objective in Eq. (13) essentially states that we want to conduct coordinate denoising, as shown in Fig. 3. Yet, this is not a trivial task due to the complicated geometric space (*e.g.*, 3D coordinates) reconstruction.

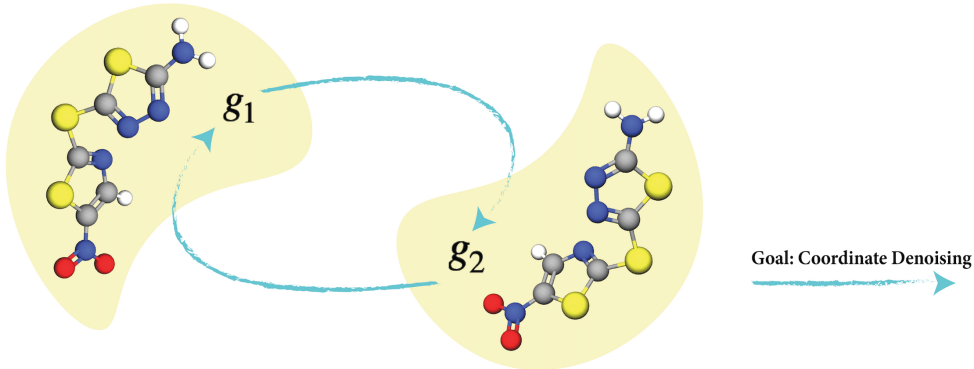


Figure 3: Pipeline for denoising coordinate matching.

C.1 An EBM framework for MI estimation

The lower bound in Eq. (13) is composed of two conditional log-likelihood terms, and then we model the conditional likelihood with EBM. This gives us:

$$\mathcal{L}_{\text{EBM}} = -\frac{1}{2} \mathbb{E}_{p(\mathbf{g}_1, \mathbf{g}_2)} \left[\log \frac{\exp(f_{g_1}(\mathbf{g}_1, \mathbf{g}_2))}{A_{g_1|\mathbf{g}_2}} + \log \frac{\exp(f_{g_2}(\mathbf{g}_2, \mathbf{g}_1))}{A_{g_2|\mathbf{g}_1}} \right], \quad (14)$$

where $f_{g_1}(\mathbf{g}_1, \mathbf{g}_2) = -E(\mathbf{g}_1 | \mathbf{g}_2)$ and $f_{g_2}(\mathbf{g}_2, \mathbf{g}_1) = -E(\mathbf{g}_2 | \mathbf{g}_1)$ are the negative energy functions, and $A_{g_1|\mathbf{g}_2}$ and $A_{g_2|\mathbf{g}_1}$ are the corresponding partition functions. The energy functions can be flexibly defined, thus the bottleneck here is the intractable partition function due to the high cardinality. To solve this, existing methods include noise-contrastive estimation (NCE) [23] and score matching (SM) [55, 56], and we will describe how to apply them for MI maximization.

C.2 EBM-NCE for MI estimation

Under the EBM framework, if we solve Eq. (14) with Noise-Contrastive Estimation (NCE) [23], the final objective is termed EBM-NCE, as:

$$\begin{aligned} \mathcal{L}_{\text{EBM-NCE}} = & -\frac{1}{2} \mathbb{E}_{p_{\text{data}}(y)} \left[\mathbb{E}_{p_n(g_1|g_2)} [\log(1 - \sigma(f_{g_1}(g_1, g_2)))] + \mathbb{E}_{p_{\text{data}}(g_1|g_2)} [\log \sigma(f_{g_1}(g_1, g_2))] \right] \\ & -\frac{1}{2} \mathbb{E}_{p_{\text{data}}(x)} \left[\mathbb{E}_{p_n(g_2|g_1)} [\log(1 - \sigma(f_{g_2}(g_2, g_1)))] + \mathbb{E}_{p_{\text{data}}(g_2|g_1)} [\log \sigma(f_{g_2}(g_2, g_1))] \right]. \end{aligned} \quad (15)$$

All the detailed derivations can be found in [23]. Specifically, EBM-NCE is equivalent to the Jensen-Shannon estimation for MI, while the mathematical intuitions and derivation processes are different. Besides, it also belongs to the contrastive SSL venue. That is, it aims at aligning the positive pairs and contrasting the negative pairs.

C.3 EBM-SM for MI estimation: SE(3)-DDM

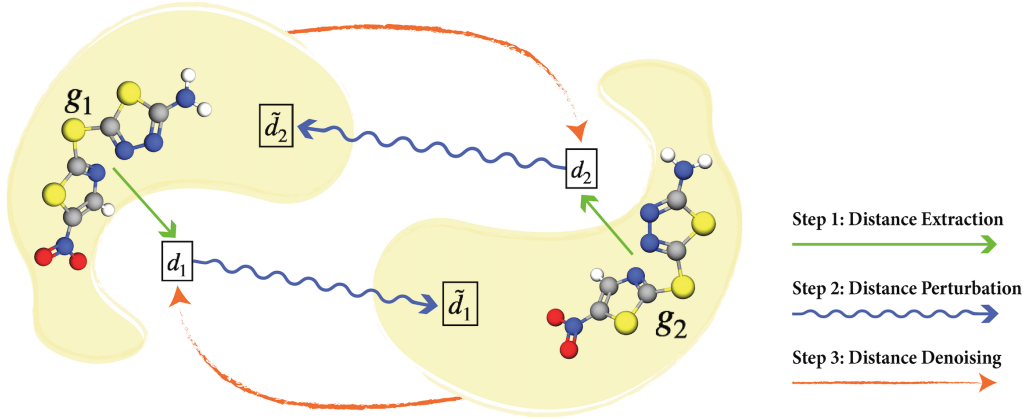


Figure 4: Pipeline for SE(3)-invariant denoising distance matching (SE(3)-DDM). The g_1 and g_2 are around the same local minima, yet with coordinate noises perturbation. Originally we want to do coordinate denoising between these two views. Then as proposed in SE(3)-DDM, we transform it to an equivalent problem, *i.e.*, distance denoising. This figure shows the three key steps: extract the distances from the two geometric views, then perform distance perturbation, and finally denoise the perturbed distances.

In this subsection, we will be focusing on the geometric data like molecular geometry. Recall that we have two views: g_1 and g_2 , and the goal is to maximize the lower bound of the mutual information in Eq. (13). Because the two views share the same atomic features, it can be reduced to:

$$\begin{aligned} \mathcal{L}_{\text{MI}} &= \frac{1}{2} \mathbb{E}_{p(g_1, g_2)} [\log p(g_1|g_2)] + \frac{1}{2} \mathbb{E}_{p(g_1, g_2)} [\log p(g_2|g_1)] \\ &= \frac{1}{2} \mathbb{E}_{p(g_1, g_2)} [\log p(\langle X_1, R_1 \rangle | \langle X_2, R_2 \rangle)] + \frac{1}{2} \mathbb{E}_{p(g_1, g_2)} [\log p(\langle X_2, R_2 \rangle | \langle X_1, R_1 \rangle)] \\ &= \frac{1}{2} \mathbb{E}_{p(g_1, g_2)} [\log p(R_1|g_2)] + \frac{1}{2} \mathbb{E}_{p(g_1, g_2)} [\log p(R_2|g_1)] \\ &= \frac{1}{2} \mathbb{E}_{p(g_1, g_2)} \left[\log \frac{\exp(f(R_1, g_2))}{A_{R_1|g_2}} \right] + \frac{1}{2} \mathbb{E}_{p(g_2, g_1)} \left[\log \frac{\exp(f(R_2, g_1))}{A_{R_2|g_1}} \right], \end{aligned} \quad (16)$$

where the $f(\cdot)$ are the negative of energy functions, and $A_{R_1|g_2}$ and $A_{R_2|g_1}$ are the intractable partition functions. The first equation in Eq. (16) results from that the two views share the same atom types. This equation can be treated as denoising the atom coordinates of one view from the geometry of the other view. In the following, we will explore how to use the score matching for solving EBM, and further transform the coordinate-aware mutual information maximization to the denoising distance matching (SE(3)-DDM) as the final objective.

Score Definition. The two terms in Eq. (3) are in the mirroring direction. Thus in what follows, we may as well adopt a proxy task that these two directions can be calculated separately, and take one direction for illustration, *e.g.*, $\log \frac{\exp(f(R_1, g_2))}{A_{R_1|g_2}}$. The score is defined as the gradient of the log-likelihood w.r.t. the data, *i.e.*, the atom coordinates in our case. Because the normalization function is a constant w.r.t. the data, it will disappear during the score calculation. To adapt it into our setting, the score is obtained as the gradient of the negative energy function w.r.t. the atom coordinates, as:

$$s(R_1, g_2) = \nabla_{R_1} \log p(R_1|g_2) = \nabla_{R_1} f(R_1, g_2). \quad (17)$$

If we assume that the learned optimal energy function, *i.e.*, $f(\cdot)$, possesses certain physical or chemical information, then the score in Eq. (17) can be viewed as a special form of the pseudo-force. This may require more domain-specific knowledge, and we leave this for future exploration.

Score Decomposition: From Coordinates To Distances. Through back-propagation [47], the score on atom coordinates can be further decomposed into the scores attached to pairwise distances:

$$\begin{aligned}
s(R_1, \mathbf{g}_2)_i &= \frac{\partial f(R_1, \mathbf{g}_2)}{\partial r_{1,i}} \\
&= \sum_{j \in \mathcal{N}(i)} \frac{\partial f(R_1, \mathbf{g}_2)}{\partial d_{1,ij}} \cdot \frac{\partial d_{1,ij}}{\partial r_{1,i}} \\
&= \sum_{j \in \mathcal{N}(i)} \frac{1}{d_{1,ij}} \cdot \frac{\partial f(R_1, \mathbf{g}_2)}{\partial d_{1,ij}} \cdot (r_{1,i} - r_{1,j}) \\
&= \sum_{j \in \mathcal{N}(i)} \frac{1}{d_{1,ij}} \cdot s(\mathbf{d}_1, \mathbf{g}_2)_{ij} \cdot (r_{1,i} - r_{1,j}),
\end{aligned} \tag{18}$$

where $s(\mathbf{d}_1, \mathbf{g}_2)_{ij} \triangleq \frac{\partial f(R_1, \mathbf{g}_2)}{\partial d_{1,ij}}$. Such decomposition has a nice underlying intuition from the pseudo-force perspective: the pseudo-force on each atom can be further decomposed as the summation of pseudo-forces on the pairwise distances starting from this atom. Note that here the pairwise atoms are connected in the 3D Euclidean space, not by the covalent-bonding.

Denoising Distance Matching (DDM). Then we adopt the denoising score matching (DSM) [64] to our task. To be more concrete, we take the Gaussian kernel as the perturbed noise distribution on each pairwise distance, *i.e.*, $q_\sigma(\tilde{\mathbf{d}}_1 | \mathbf{g}_2) = \mathbb{E}_{p_{\text{data}}(\mathbf{d}_1 | \mathbf{g}_2)} [q_\sigma(\tilde{\mathbf{d}}_1 | \mathbf{d}_1)]$, where σ is the deviation in Gaussian perturbation. One main advantage of using the Gaussian kernel is that the following gradient of conditional log-likelihood has a closed-form formulation: $\nabla_{\tilde{\mathbf{d}}_1} \log q_\sigma(\tilde{\mathbf{d}}_1 | \mathbf{d}_1, \mathbf{g}_2) = (\mathbf{d}_1 - \tilde{\mathbf{d}}_1) / \sigma^2$, and the goal of DSM is to train a score network to match it. This trick was first introduced in [64], and has been widely utilized in the score matching applications [53, 54].

To adapt this into our setting, this is essentially saying that we want to train a ‘‘distance network’’, *i.e.*, $s_\theta(\tilde{\mathbf{d}}_1 | \mathbf{g}_2)$, to match the distance perturbation, or we can say it aims at matching the pseudo-force with the pairwise distances from another aspect. By taking the Fisher divergence as the discrepancy metric and the trick mentioned above, the estimation $s_\theta(\tilde{\mathbf{d}}_1, \mathbf{g}_2) \approx \nabla_{\tilde{\mathbf{d}}_1} \log q(\tilde{\mathbf{d}}_1 | \mathbf{d}_1, \mathbf{g}_2)$ can be simplified to the following:

$$D_F(q_\sigma(\tilde{\mathbf{d}}_1 | \mathbf{g}_2) || p_\theta(\tilde{\mathbf{d}}_1 | \mathbf{g}_2)) = \frac{1}{2} \mathbb{E}_{p_{\text{data}}(\mathbf{d}_1 | \mathbf{g}_2)} \mathbb{E}_{q_\sigma(\tilde{\mathbf{d}}_1 | \mathbf{d}_1, \mathbf{g}_2)} \left[\left\| s_\theta(\tilde{\mathbf{d}}_1, \mathbf{g}_2) - \frac{\mathbf{d}_1 - \tilde{\mathbf{d}}_1}{\sigma^2} \right\|^2 \right] + C. \tag{19}$$

Final objective. We adopt the following four model training tricks from [34, 53, 54] to stabilize the score matching training process. (1) We carry out the distance denoising at L -level of noises. (2) We add a weighting coefficient $\lambda(\sigma) = \sigma^\beta$ for each noise level, where β is the annealing factor. (3) We scale the score network by a factor of $1/\sigma$. (4) We sample the exactly same atoms from the two geometry views with masking ratio r . Finally, by considering the two directions and all the above tricks, the objective function becomes the follows:

$$\begin{aligned}
\mathcal{L}_{\text{SE(3)-DDM}} &= \frac{1}{2L} \sum_{l=1}^L \sigma_l^\beta \mathbb{E}_{p_{\text{data}}(\mathbf{d}_1 | \mathbf{g}_2)} \mathbb{E}_{q(\tilde{\mathbf{d}}_1 | \mathbf{d}_1, \mathbf{g}_2)} \left[\left\| \frac{s_\theta(\tilde{\mathbf{d}}_1, \mathbf{g}_2)}{\sigma_l} - \frac{\mathbf{d}_1 - \tilde{\mathbf{d}}_1}{\sigma_l^2} \right\|_2^2 \right] \\
&\quad + \frac{1}{2L} \sum_{l=1}^L \sigma_l^\beta \mathbb{E}_{p_{\text{data}}(\mathbf{d}_2 | \mathbf{g}_1)} \mathbb{E}_{q(\tilde{\mathbf{d}}_2 | \mathbf{d}_2, \mathbf{g}_1)} \left[\left\| \frac{s_\theta(\tilde{\mathbf{d}}_2, \mathbf{g}_1)}{\sigma_l} - \frac{\mathbf{d}_2 - \tilde{\mathbf{d}}_2}{\sigma_l^2} \right\|_2^2 \right].
\end{aligned} \tag{20}$$

C.4 Discussions

Using the energy-based model (EBM) to solve MI maximization can open a novel venue, especially for high-structured data like molecular geometry. To solve EBM, existing methods include noise-contrastive estimation (NCE) [23], score matching (SM) [56], etc. To put this under the MI maximization setting, EBM-NCE is essentially a contrastive learning method, where the goal is to align the positive pairs and contrast the negative pairs simultaneously. While EBM-SM or SE(3)-DDM is a generative self-supervised learning (SSL) on distance denoising, and it is especially appealing in the field for geometric data representation learning.

Score matching can be smoothly adopted to 3D geometric setting. Because scores are defined as gradients of the energy function with respect to the atom positions, it can be thought of a form of pseudo-forces. Following this, SE(3)-DDM can be viewed as a pseudo-force matching, which is more natural to the molecular structures. However, further understanding of this requires more domain knowledge in understanding or designing of the energy function. This is beyond the score of this paper, and we would like to leave it for future exploration.

Recently, there have been a certain works [34] proving that 3D geometric information is useful for 2D topology. Here we want to conjecture that the reverse direction is also meaningful: 2D topology can be also useful for 3D representation. This may not seem reasonable from the domain perspective, since 2D topology can be heuristically obtained from the 3D geometry, *i.e.*, all the 2D information is redundant to 3D geometry. However, from the machine learning theory perspective [4, 17], this is still helpful in reducing the sample complexity. From a higher level perspective, we want to explicitly point out that such gap between machine learning and scientific domain has been widely existed, and it would be an interesting direction for further exploration.

D Experiments

In this section, we would like to discuss the experiment details of our work. The main structure is as follows:

- In Appendix D.1, we introduce the computation resources.
- Appendices D.2 to D.4, we introduce the downstream datasets.
 - Notice that because the performance of QM9 and MD17 is quite stable after fixing the seed (*e.g.*, 42), we will not run cross-validation. This also follows the main literature [36, 45, 46].
 - Yet, for LBA & LEP, these two datasets are quite small and are very sensitive to the data splitting, so we pick up 5 seeds (12, 22, 32, 42, and 52) and run cross validation.
- In Appendix D.5, we list the key hyperparameters for all the pretraining baselines and SE(3)-DDM.
- In Appendix D.6, we show the empirical results using SchNet as the backbone model.

D.1 Computational Resources

We have 20 V100 GPU cards for computation at an internal cluster. Each job can be finished within 3-24 hours.

D.2 Dataset: QM9

QM9 [41] is a dataset of 134K molecules consisting of 9 heavy atoms. It includes 12 tasks that are related to the quantum properties. For example, U0 and U298 are the internal energies at 0K at 0K and 298.15K respectively, and U298 and G298 are the other two energies that can be transferred from H298 respectively. The other 8 tasks are quantum mechanics related to the DFT process. We follow [45] in preprocessing the dataset (including unit transformation for each task).

Current work is using different different data split (in terms of the splitting size). Originally there are 133,885 molecules in QM9, where 3,054 are filtered out, leading to 130,831 molecules. During the benchmark, we find that the performance on QM9 is very robust to either using (1) 110K for training, 10K for val, 10,831 for test or using (2) 100K for training, 13,083 for val and 17,748 for test. In this paper, we are using option (1).

D.3 Dataset: MD17

MD17 [9] is a dataset on molecular dynamics simulation. It includes eight tasks, corresponding to eight organic molecules, and each task includes the molecule positions along the potential energy surface (PES), as shown in Fig. 1. The goal is to predict the energy-conserving interatomic forces for each atom at each molecule position. We list some basic statistics in Table 6. We follow [36, 46] in preprocessing the dataset (including unit transformation for each task).

Table 6: Some basic statistics on MD17.

Pretraining	Aspirin ↓	Benzene ↓	Ethanol ↓	Malonaldehyde ↓	Naphthalene ↓	Salicylic ↓	Toluene ↓	Uracil ↓
Train	1K	1K	1K	1K	1K	1K	1K	1K
Validation	1K	1K	1K	1K	1K	1K	1K	1K
Test	209,762	47,863	553,092	991,237	324,250	318,231	440,790	131,770

D.4 Dataset: LBA & LEP

Atom3D [61] is a newly published dataset. It gathers several core tasks for 3D molecules, including binding affinity. The binding affinity prediction is to measure the strength of binding interaction between a small molecule to the target protein. Here we will model both the small molecule and large molecule (protein) with their 3D atom coordinates provided.

Table 7: Some basic statistics on LBA & LEP. For LBA, we use split-by-sequence-identity-30: we split protein-ligand complexes such that no protein in the test dataset has more than 30% sequence identity with any protein in the training dataset. For LEP, we split the complex pairs by protein target.

	Pretraining	LBA	LEP
Train		3,507	304
Validation		466	110
Test		490	104
Split	split-by-identity-30	split-by-target	

During the binding process, there is a cavity in a protein that can potentially possess suitable properties for binding a small molecule (ligand), and it is termed a pocket [57]. Because of the large volume of protein, we follow [61] by only taking the binding pocket, where there are no more than 600 atoms for each molecule and

protein pair. To be more concrete, we consider two binding affinity tasks. (1) The first task is ligand binding affinity (LBA). It is gathered from [65] and the task is to predict the binding affinity strength between a small molecule and a protein pocket. (2) The second task is ligand efficacy prediction (LEP). The input is a ligand and both the active and inactive conformers of a protein, and the goal is to predict whether or not the ligand can activate the protein’s function. We list some basic statistics in Table 7.

D.5 Hyperparameter Specification

We list all the detailed hyperparameters in this subsection. For all the methods, we use the same optimization strategy, *i.e.*, with learning rate as 5e-4 and cosine annealing learning rate schedule [38]. The other hyperparameters for each pretraining method are listed in Table 8. For the other hyperparameters, we are using the default hyperparameters, as attached in the codes.

Table 8: Hyperparameter specifications.

Pretraining	Hyperparameter	Value
Supervised	task	{total energy}
Type Prediction	masking ratio	{0.15, 0.3}
Distance Prediction	prediction rate	{1}
Angle Prediction	prediction rate	{1e-3, 1e-4}
RR	perturbed noise μ	{0}
	perturbed noise σ	{0.3}
	masking ratio r	{0, 0.3}
InfoNCE	perturbed noise μ	{0}
	perturbed noise σ	{0.3, 1}
	masking ratio r	{0, 0.3}
EBM-NCE	perturbed noise μ	{0}
	perturbed noise σ	{0.3, 1}
	masking ratio r	{0, 0.3}
SE(3)-DDM	perturbed noise μ	{0}
	perturbed noise σ	{0.3}
	masking ratio r	{0, 0.3}
	L	{30, 50}
	σ_1	{0.01}
	σ_L	{10}
	annealing factor β	{0.05, 0.2, 2, 5, 10}

D.6 SchNet as Backbone Model

We want to highlight that some backbone models (*e.g.*, DimeNet++ and SphereNet) may perform better or on par with the PaiNN, as shown in Table 4. Yet they will be out of GPU memory. Thus, considering all (including the model performance, computation efficiency, and memory cost) together, we adopt PaiNN as the backbone model in the main paper.

In this section, we carry out experiments using SchNet as the backbone model. We follow the same process as in Sec. 5, *i.e.*, we compare our method with one randomly-initialized and seven pretraining baselines. The results on QM9, MD17, LBA and LEP are in Tables 9 to 11 accordingly. From these three tables, we can observe that in general, SE(3)-DDM can reach the most optimal results, yielding 21 best performance in 22 downstream tasks, and can reach comparative performance on the remaining task (within top 2 model). This can largely support the effectiveness of our proposed method, SE(3)-DDM. In addition, we also want to mention that a lot of pretraining tasks show the negative transfer issue. Comparing to the results in Sec. 5, we conjecture that this is related to the task (both pretraining and downstream tasks) and the backbone model. Yet, this is beyond the scope of our work, and we would like to leave this as a future direction.

Table 9: Downstream results on 12 quantum mechanics prediction tasks from QM9. We take 110K for training, 10K for validation, and 11K for test. The evaluation is mean absolute error, and the best results are in **bold**.

Pretraining	Alpha ↓	Gap ↓	HOMO ↓	LUMO ↓	Mu ↓	Cv ↓	G298 ↓	H298 ↓	R2 ↓	U298 ↓	U0 ↓	Zpve ↓
–	0.070	50.59	32.53	26.33	0.029	0.032	14.68	14.85	0.122	14.70	14.44	1.698
Supervised	0.070	51.34	32.62	27.61	0.030	0.032	14.08	14.09	0.141	14.13	13.25	1.727
Type Prediction	0.084	56.07	34.55	30.65	0.040	0.034	18.79	19.39	0.201	19.29	18.86	2.001
Distance Prediction	0.068	49.34	31.18	25.52	0.029	0.032	13.93	13.59	0.122	13.64	13.18	1.676
Angle Prediction	0.084	57.01	37.51	30.92	0.037	0.034	15.81	15.89	0.149	16.41	15.76	1.850
RR	0.073	52.57	34.44	28.41	0.033	0.038	15.74	16.11	0.194	15.58	14.76	1.804
InfoNCE	0.075	53.00	34.29	27.03	0.029	0.033	15.67	15.53	0.125	15.79	14.94	1.675
EBM-NCE	0.073	52.86	33.74	28.07	0.031	0.032	14.02	13.65	0.121	13.70	13.45	1.677
SE(3)-DDM (ours)	0.066	48.59	30.83	25.27	0.028	0.031	13.06	12.33	0.117	12.48	12.06	1.631

Table 10: Downstream results on 8 force prediction tasks from MD17. We take 1K for training, 1K for validation, and the number of molecules for test are varied among different tasks, ranging from 48K to 991K. The evaluation is mean absolute error, and the best results are in **bold**.

Pretraining	Aspirin ↓	Benzene ↓	Ethanol ↓	Malonaldehyde ↓	Naphthalene ↓	Salicylic ↓	Toluene ↓	Uracil ↓
–	1.196	0.404	0.542	0.879	0.534	0.786	0.562	0.730
Supervised	1.863	0.413	0.512	1.254	0.846	1.005	0.529	0.899
Type Prediction	1.293	0.787	0.547	0.879	1.030	1.076	0.614	0.738
Distance Prediction	1.414	0.453	0.845	1.371	0.591	0.819	0.588	0.993
Angle Prediction	3.030	0.450	0.485	0.845	1.112	1.214	0.791	1.016
RR	1.878	0.450	0.690	2.255	0.960	1.382	0.784	1.188
InfoNCE	1.286	0.396	0.512	1.007	0.778	1.060	0.667	0.933
EBM-NCE	1.271	0.400	0.570	0.972	0.605	0.862	0.576	0.790
SE(3)-DDM (ours)	1.176	0.368	0.434	0.779	0.460	0.700	0.561	0.679

Table 11: Downstream results on 2 binding affinity prediction tasks. We select three evaluation metrics for LBA: the root mean squared error (RMSD), the Pearson correlation (R_P) and the Spearman correlation (R_S). LEP is a binary classification task, and we use the area under the curve for receiver operating characteristics (ROC) and precision-recall (PR) for evaluation. We run cross validation with 5 seeds, and the best results are in **bold**.

Pretraining	LBA			LEP	
	RMSD ↓	R_P ↑	R_C ↑	ROC ↑	PR ↑
–	1.489 ± 0.02	0.522 ± 0.01	0.501 ± 0.01	0.436 ± 0.03	0.369 ± 0.02
Supervised	1.477 ± 0.04	0.528 ± 0.02	0.503 ± 0.03	0.462 ± 0.05	0.392 ± 0.03
Type Prediction	1.483 ± 0.04	0.498 ± 0.03	0.481 ± 0.03	0.570 ± 0.04	0.509 ± 0.07
Distance Prediction	1.461 ± 0.06	0.535 ± 0.04	0.512 ± 0.04	0.502 ± 0.06	0.415 ± 0.05
Angle Prediction	1.499 ± 0.01	0.475 ± 0.01	0.462 ± 0.02	0.532 ± 0.06	0.449 ± 0.03
RR	–	–	–	0.439 ± 0.04	0.365 ± 0.02
InfoNCE	1.528 ± 0.05	0.483 ± 0.02	0.464 ± 0.02	0.588 ± 0.06	0.523 ± 0.05
EBM-NCE	1.499 ± 0.03	0.509 ± 0.02	0.498 ± 0.02	0.493 ± 0.07	0.429 ± 0.06
SE(3)-DDM (ours)	1.432 ± 0.02	0.550 ± 0.02	0.529 ± 0.02	0.633 ± 0.03	0.541 ± 0.03